# A methodology for the calibration of the effective stress parameter : From macroscopic considerations to microstructural validation

*Hesam* Ebrahimisadr[1,*], *Sophie* Lanckohr[1], and *Bertrand* Francois[1]

[1]Université de Liège, ArGEnCo Department, Allée de la Découverte, 9 - 4000 Liège, Belgium

**Abstract.** This study proposes an experimental methodology to calibrate the effective stress parameter χ for unsaturated soils, ensuring a unique shear failure criterion. The study integrates water retention behaviour and shear strength to calibrate the χ parameter through an experimental method. The experimental study was conducted on a reconstituted clayey soil with a plasticity index of 98.3%. Unconfined compression tests were conducted under six suction levels (5 controlled RH, and laboratory conditions) to assess soil strength and stiffness. Triaxial consolidated undrained tests were performed on saturated samples to determine the intrinsic failure criterion. Then, combining uniaxial compression strength (UCS) at various suctions and shear failure criterion under saturated conditions, the χ parameter was calculated for different suction levels. Finally, a power law equation relating χ parameter to the degree of saturation is calibrated. This method ensures that the Mohr-Coulomb failure criterion remains consistent, regardless of suction conditions. In this approach, the strength gain observed at high suction is integrated in the effective stress formulation. At the end of the study, the calibration is validated from microstructural considerations. From pore size distribution obtained by mercury intrusion porosimetry, it is demonstrated that the χ parameter is essentially affected by the water retention properties of macro-porosity while the water retention of micro-porosity has no effect on the macroscopic effective stress.

## 1 Introduction

Unsaturated soils display complex mechanical behavior due to the coexistence of air and water in their pore network. This results in pore pressures and surface tensions which affect the overall stress-strain response. Unlike saturated soils, where effective stress is well-defined, unsaturated soils require additional considerations to account for suction and water retention properties [1].

Terzaghi's principle of effective stress [2]states that all measurable effects of stress, such as compaction and shear resistance, should be attributed to changes in effective stress. In unsaturated soils, suction affects stress transmission at the particle level, influencing macroscopic behavior. The degree of saturation plays a crucial role in determining how suction contributes to effective stress, especially in clays, which exhibit strong hydro-mechanical coupling due to their high water retention capacity.

Bishop [3] introduced a generalized effective stress framework incorporating the effective stress parameter, χ, which adjusts the influence of suction based on the degree of saturation. (Eq. 1)

$$\sigma'_{ij} = \sigma_{ij} + \chi s \delta_{ij} \quad (1)$$

Various studies [4–12] have proposed empirical relationships between χ and the degree of saturation or suction, considering, for some of them, factors like pore size distribution and interfacial forces.

This study presents an experimental methodology to calibrate the χ parameter using a unique shear failure criterion. The method combines uniaxial compression tests at different suctions with triaxial compression tests under saturated conditions. By ensuring a consistent Mohr-Coulomb failure criterion across various suction levels, the study refines the relationship between χ and degree of saturation. Additionally, microstructural analysis via mercury intrusion porosimetry (MIP) highlights the roles of micro- and macro-porosity in effective stress transmission.

## 2 Materials and methods

### 2.1. Material

A high-plastic soil is studied in this research. It is called "Tournai" corresponding to the location where it has been extracted in Belgium. To characterize the material, particle size analysis, Atterberg limits, and the standard

* Corresponding author: h.ebrahimisadr@uliege.be

Proctor tests were performed (Table 1). 88.5% of the grains have a diameter smaller than 80 µm.

**Table 1.** Mechanical properties of the Tournai soil.

| | |
|---|---|
| Liquid Limit (%) | 141.1 |
| Plastic Limit (%) | 42.76 |
| Shrinkage Limit (%) | 27 |
| Plasticity Index (%) | 98.3 |
| Soil type (USCS) | CH |
| Maximum dry Unit Weight under standard proctor compaction (g/cm³) | 1.04 |
| Optimum Water Content under standard proctor compaction (%) | 47.6 |
| Initial Degree of Saturation under as-compacted state (%) | 85 |
| Matric suction under as-compacted state (*) (MPa) | 1.063 |
| Total suction under as-compacted state (*) (MPa) | 1.351 |

(*) Measured from the filter paper method according to [13]

Samples were prepared by static compaction at optimum standard Proctor conditions (water content and dry density). The soil was mixed with the optimum water content, sealed in a plastic bucket to homogenize moisture for at least 24 hours, and stored inverted to rest on its lid to minimize moisture loss. Specimens were then statically compacted into cylindrical molds.

### 2.2 Experimental methods

The saline-solution method was used to impose various relative humidity (RH), leading to various suctions, as detailed in [14]. This technique aims to impose suctions from 4.2 MPa to 110 MPa. Furthermore, the mass was measured after compaction, after hydric equilibrium and after full drying in an oven at 105°C to deduce the water content and the degree of saturation and plot the water retention curve. Then, the water retention curve was fitted with the Van Genuchten method [15].

$$S_r = \left[1+\left(\frac{s}{P_r}\right)^n\right]^{\left(\frac{1}{n}-1\right)} \quad (2)$$

The curve is calibrated on the experimental points to obtain the best matching in the sense of the least square method.

Uniaxial compression tests were performed at a rate of 0.3 mm/min on the specimen under six suction level conditions (five controlled relative humidity and the laboratory condition).

Triaxial compression tests, under 100 kPa, 200 kPa and 400 kPa of confining pressure, were performed on saturated soil specimens under consolidated undrained conditions to deduce the intrinsic shear failure criterion.

## 3 Experimental Results

### 3.1 Triaxial CU test

The effective cohesion (c) of 21.8 Kpa, and friction angle ($\phi$) of 21.6 ° is obtained from consolidated undrained (CU) triaxial compression tests under saturated conditions. Mohr circles at failure are plotted in Fig. 1, while Figs. 2, 3 and 4 represent the stress path in mean effective stress ($p'$) vs deviatoric stress ($q$) plane, pore water pressure vs axial strain and deviatoric stress vs axial strain, respectively. The selected failure criterion corresponds to the conditions when the axial stress is maximum.

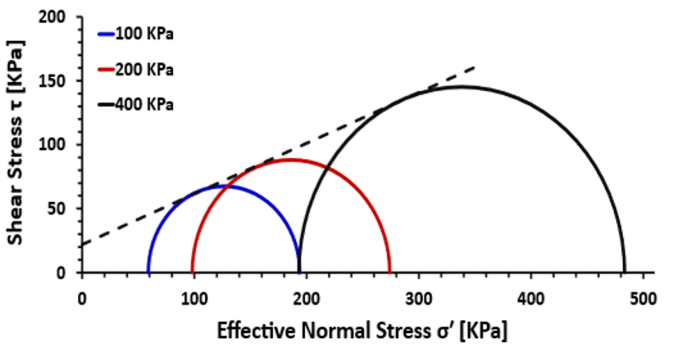


**Fig. 1.** Shear stress vs. effective normal stress.

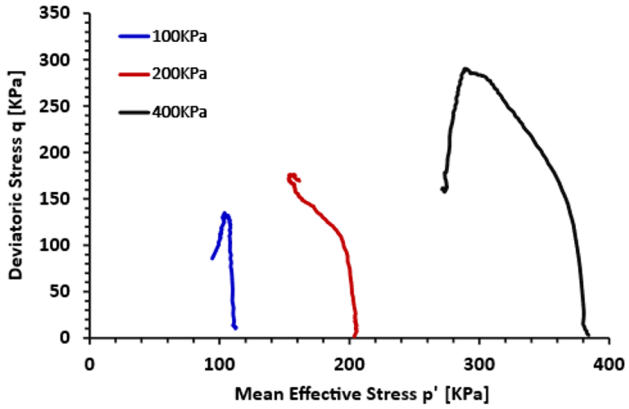


**Fig. 2.** Stress paths in p'-q space.

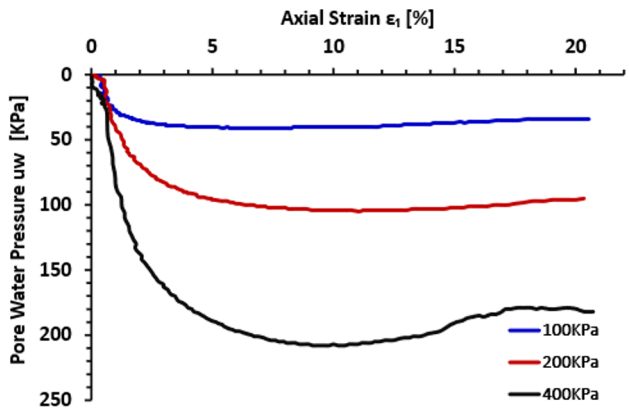


**Fig. 3.** Pore water pressure vs. axial strain.

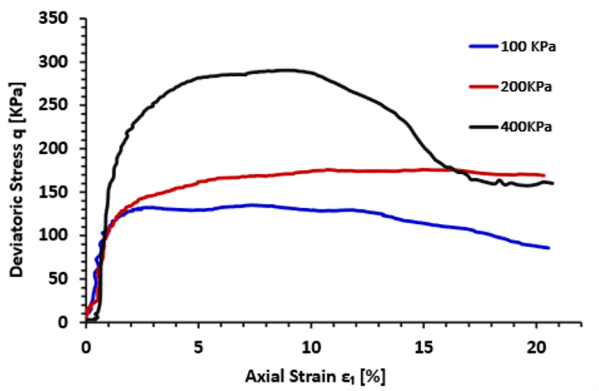


**Fig. 4.** Deviatoric stress vs. axial strain.

### 3.2 Water retention curve

The water retention curve calibrated by the van Genuchten equation is represented in Fig. 5. The calibration parameters of 0.46177 MPa for $P_r$, and 1.13 for $n$ are derived, according to Equation (2). The low slope of the curve reveals the high retention capacity which is consistent with the high plasticity index of the soil.

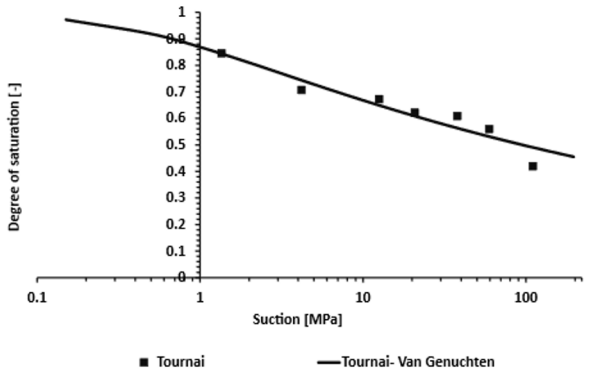


**Fig. 5.** Water retention curve.

### 3.3 Uniaxial compression test (UCS)

Uniaxial compression tests at various suctions (from 4.2 MPa to 110 MPa of suction) were conducted. Young's modulus and uniaxial compression strengths (UCS) are plotted as a function of suction in Fig.6. Young's modulus is determined as the maximum slope of the axial stress *vs* axial strain curve on an axial strain interval of 0.2%, while the uniaxial compression strength (UCS) is the maximum axial stress reached at the peak of the curve.

## 4 Calibration of the χ parameter

The expression of the χ parameter as a function of the degree of saturation can be fitted through the calibration of the $\alpha$ exponent.

$$\chi = (S_r)^{\alpha} \quad (3)$$

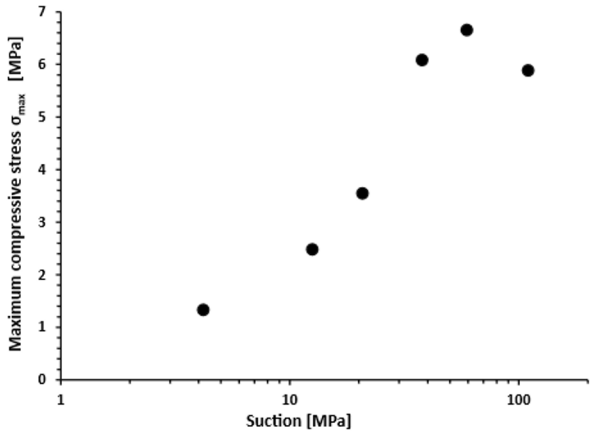


(a)

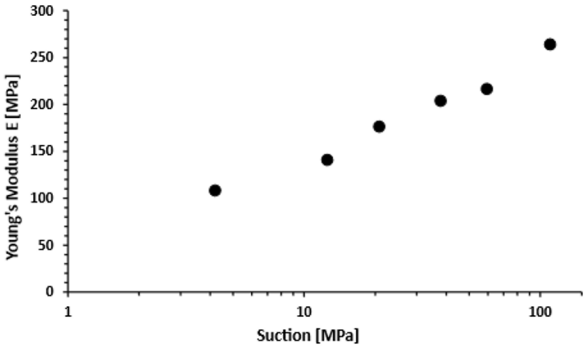


(b)

**Fig. 6.** Evolution of (a) uniaxial compressive strength and (b) Young's modulus; as a function of suction.

The main principle is to target the uniqueness of the shear failure criterion whatever the suction level, when the stress state is expressed in the generalized effective stress reference, according to the methodology developed by [16].

The $\alpha$ exponent is a material parameter which is the slope of the regression line in the $(log\, S_r\, ;\, log\, \chi)$ plane.

$$log\, \chi = \alpha\, log\, S_r \quad (4)$$

For every single test result (at one suction and one degree of saturation), one value of χ can be deduced. So, it is possible to obtain a set of points in the $(log\, S_r\, ;\, log\, \chi)$ plane and then find the best regression line, with the slope being the $\alpha$ parameter. From this curve, the best fit obtained for $\alpha$ is 3.97 (Fig.7).

The set of Mohr circles at failure obtained from uniaxial compression at various suctions is illustrated in Fig. 8, using the generalized effective stress. As expected, by the essence of the methodology, the obtained Mohr circles at failure tend to align on a unique failure criterion based on the cohesion and the friction angle deduced from the triaxial test.

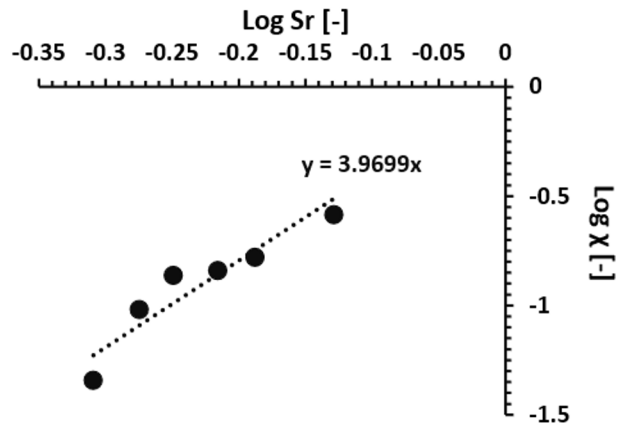


**Fig. 7.** Calibration of the $\alpha$ exponent as the slope of the linear regression curve in the $(log\ S_r; log\ \chi)$ plane.

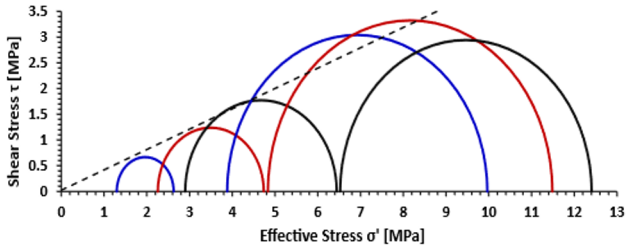


**Fig. 8.** Mohr circles at failure expressed in terms of generalized effective stress for uniaxial compression tests performed at different initial suctions.

## 5 Mercury intrusion porosimetry (MIP)

The evolution of the effective stress parameter χ in unsaturated soils is fundamentally linked to the underlying microstructural changes occurring within the pore network. According to the concept developed by [10] subsequently adapted by [8], [9] and [7], only the ‘‘inter-aggregate’’ water (located in macro-voids) contributes to the macroscopic effective stress, while the ‘‘intra-aggregate’’ water (located in micro-voids) is neutral regarding the χ parameter. This concept is described by the following equation

$$\chi = \frac{S_r - S_r^m}{1 - S_r^m} \tag{5}$$

where $S_r^m$ is the microstructural degree of saturation that refers to the degree of saturation needed to fully saturate the micro-porosity while the macro-porosity remains dry. Fig. 9 illustrates Eq. 5 for different values of $S_r^m$ and compares it with Eq. 1 for different values of $\alpha$.

As long as the water is confined within aggregates there is no evolution of χ. Once aggregates become fully saturated, additional water migrates into larger voids, leading to capillary effects between aggregates that cause an increase in χ.

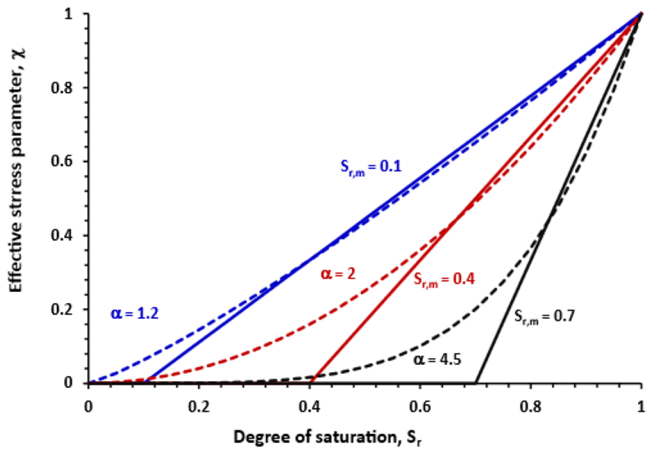


**Fig. 9.** Comprehensive justification of the power law based on microstructural features.

Consequently, the pore size distribution (PSD) is a good indicator of the relation between the χ parameter and the degree of saturation. Fig. 10 shows the pore size distribution at the initial state (before any suction application) obtained from mercury intrusion porosimetry (MIP). Differentiation between micro- and macro-porosity is delimited by the lowest point of the PSD at intermediate pore diameter.

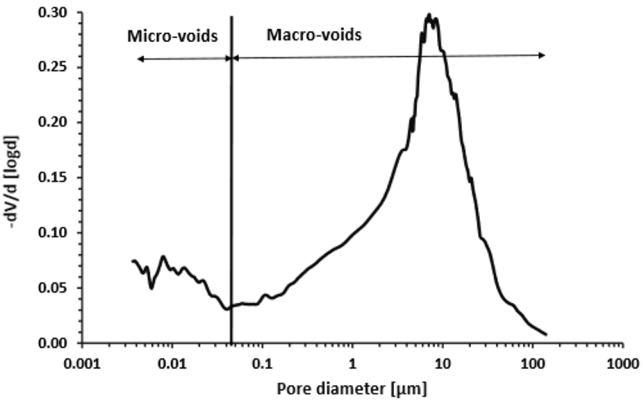


**Fig. 10.** Pore size distribution (PSD) obtained from mercury intrusion porosimetry (MIP).

**Table 2.** Microstructural parameters deduced from mercury intrusion porosimetry (MIP).

| | |
|---|---|
| Intruded porosity | 0.472 |
| Intruded micro-porosity | 0.069 |
| Intruded macro-porosity | 0.402 |
| Total porosity | 0.587 |
| Total micro-porosity | 0.185 |
| Total macro-porosity | 0.402 |
| Total void ratio | 1.421 |
| Total micro-void ratio | 0.447 |
| Total macro-void ratio | 0.974 |
| Initial microstructural degree of saturation $S_{r,0}^m$ | 0.229 |

During suction application, the shrinkage is assumed to be fully attributed to macro-void ratio reduction. In this

concept, the aggregates (including micro-voids) are assumed incompressible while the closure of macro-voids induces macroscopic shrinkage. Consequently, upon drying, macro-voids decrease while micro-voids remain constant, as reported in Fig. 11.

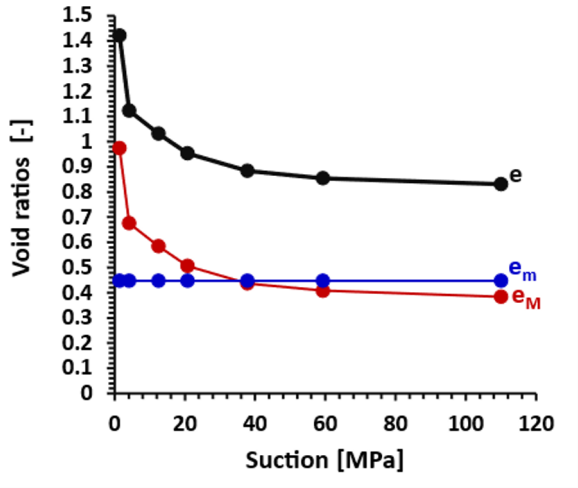


**Fig. 11.** Evolution of total void ratio (e), macro void ratio ($e_M$) and micro-void ratio ($e_m$) during drying, assuming that the micro-void ratio (intra-aggregate) remains constant.

When total, micro and macro void ratios are known at various suctions, it is then possible to deduce the χ parameter according to the concept of Eq. (5). Fig. 12 illustrates the χ parameter as a function of the degree of saturation, following four methods:

1. The value of χ such that the shear failure obtained from uniaxial compression tests at various suctions aligns with the failure criterion under saturated conditions.
2. The power law (Eq. (3)) with the $\alpha$ exponent calibrated according to the methodology developed in Section 4. From this curve, the best fit for α is 3.97 (Fig.7).
3. Eq. (5) assuming that the void ratio remains constant upon drying (i.e. $S_r^m = S_{r,0}^m = \text{constant}$)
4. Eq. (5) considering evolving void ratio upon drying as shown in Fig. 11, the reduction of the void ratio being fully attributed to the reduction of macro void ratios (i.e. $S_r^m$ increases upon drying).

Considering method (1), the relation of χ with $S_r$ is in relatively good agreement with the conceptual model of [10] based on microstructure. χ parameter remains negligible at low degrees of saturation, as water is primarily retained within the intra-aggregate microporosity. Method (2) fits relatively well the experimental point of the χ parameter. For method (3), which neglects the evolution of the microstructure upon drying, the transition between dry macro-voids and water invading macro-voids is probably too sharp. In reality, the transition between those two states is smoother because water starts to invade progressively the macro-voids while micro-voids are not yet fully saturated. Also, assuming a constant microstructure upon drying is a too strong assumption because it underestimates the $S_r^m$ parameters at the high suction. Indeed, at high suction, the macro voids have been significantly reduced, due to shrinkage, leading to a larger proportion of micro-voids over the total voids. Finally, method (4) gives a better trend than method (3) even if the transition between dry and water invading macro-voids is still too sharp for the same reason as method (3).

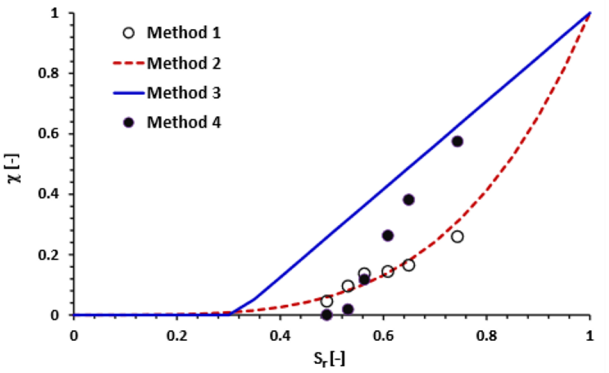


**Fig. 12.** Effective stress parameter as a function of the degree of saturation.

## 5 Conclusion

Using a generalized effective stress formulation for unsaturated soils requires calibrating the effective stress parameter χ. In this study, χ is expressed as a power law of the degree of saturation. Triaxial compression tests under saturated conditions defined the effective cohesion and friction angle. Then, uniaxial compression tests at various suctions (corresponding to various degrees of saturation) were used to find one value of χ per value of degree of saturation, to shift the uniaxial compression strength onto the intrinsic failure criterion expressed in effective stress. Finally, the power law was calibrated to best-fit χ values against degrees of saturation.

The exponent of the power law controls the rate at which the χ parameter increases with the degree of saturation. Upon a low degree of saturation, when the water is essentially stored in the micro-porosity, the χ parameter is insignificant because this "intra-aggregate" water does not contribute to the macroscopic stress. On the contrary, upon a higher degree of saturation, water floods the ''inter-aggregate'' voids, contributing more to the increase of the effective stress (i.e. χ becomes significant).

This behavior was further explored through microstructural analysis using mercury intrusion porosimetry, emphasizing the bi-modal pore structure. When the degree of saturation remains below the level needed to fill micropores, the χ parameter stays negligible. However, once saturation exceeds this threshold, the water fills macropores, and χ increases significantly. The proposed approach provides a straightforward and effective protocol to calibrate χ, relying on the assumption of a unique shear failure criterion defined in generalized effective stress terms.

## References

[1]. N. Khalili, R. Witt, L. Laloui, L. Vulliet, and A. Koliji, Geophys Res Lett **32**, (2005).

[2]. K. Terzaghi, *Theoretical Soil Mechanics* (Wiley, New York, 1936).

[3]. W. Bishop, Teknisk Ukeblad **39**, 859 (1959).

[4]. N. Khalili and M. H. Khabbaz, Géotechnique **48**, 681 (1998).

[5]. B. A. Schrefler, *The Finite Element Method in Soil Consolidation (with Applications to Surface Subsidence)*, Ph.D. Thesis, Univ. College of Swansea, 1984.

[6]. B. Kim, S. Shibuya, S.-W. Park, and S. Kato, Canadian Geotechnical Journal **47**, 955 (2010).

[7]. J. Vaunat and F. Casini, in *Poromechanics VI* (American Society of Civil Engineers, Reston, VA, 2017), pp. 1443–1450.

[8]. E. Alonso, J. M. Pereira, J. Vaunat, and S. Olivella, Geotechnique **60**, 913 (2010).

[9]. E. Alonso, N. M. Pinyol, and A. Gens, Géotechnique **63**, 463 (2013).

[10]. A. Tarantino and S. Tombolato, Géotechnique **55**, 307 (2005).

[11]. E. Nikooee, G. Habibagahi, S. M. Hassanizadeh, and A. Ghahramani, Transp Porous Media **96**, 369 (2013).

[12]. Y. Kohgo, M. Nakano, and T. Miyazaki, Soils and Foundations **33**, 49 (1993).

[13]. ASTM International, *D5298-10 Standard Test Method for Measurement of Soil Potential (Suction) Using Filter Paper* (ASTM International, West Conshohocken, PA, 2010).

[14]. P. Delage, M. D. Howat, and Y. J. Cui, Eng Geol **50**, 31 (1998).

[15]. M. Th. Van Genuchten, Soil Science Society of America Journal **44**, 892 (1980).

[16]. P. Gerard, M. Mahdad, A. Robert McCormack, and B. François, Constr Build Mater **95**, 437 (2015).